An analysis of photonic interconnect schemes for neutral atom quantum computing modules

memQ Team
Chicago, IL 60615
Contact: Sean Sullivan, CTO, sean@memq.tech

About memQ

Founded in 2022 as a technology spin-out from the University of Chicago, memQ is dedicated to enabling the scalable implementation of quantum computing through standards-based connectivity across optical connections between quantum computers anywhere. The company's portfolio provides secure connectivity and control across local, campus, metro, and wide-area quantum compute resources, optimizing for high-fidelity and low-loss, regardless of qubit structures employed. More information is available at www.memq.tech.

Executive summary

We review approaches to achieve high-rate entanglement photonic entanglement (>10 kHz) between atoms in two separate quantum computing modules in a datacenter-like scheme. Emissive qubit schemes are discussed, as these are most amenable to broad implementation in a qubit-agnostic and extensible network architecture.

The first approach is direct entanglement by performing a Bell state measurement (BSM) on the emitted photons from the two atoms. Here, entanglement rates of 30 Hz have been demonstrated on cavity coupled neutral atoms, with potential improvement to 3-5 kHz proposed under this scheme. The second approach, asynchronous BSM, uses intermediate quantum memories to increase entanglement rates in a regime where the photon collection is non-deterministic due to low collection efficiency. Given state-of-the-art photon collection efficiencies (>0.01), introduction of optimal quantum memories can lead to ~100x enhancement of entanglement rates in this photon-starved regime, with decreasing enhancement as photon collection efficiencies are improved.

Multiplexing across several atoms, specifically time-multiplexing leveraging the ability to trap arrays with 100s of atoms could provide a route towards high-rate entanglement. Entanglement rates in excess of 100 kHz have been proposed under this scheme.

1. Introduction

In order to build utility-scale quantum computers, we need to network quantum computer modules in a data center-like setting, also referred to as the ***quantum data center***. Optical interconnect schemes are one of the most promising approaches for interconnecting smaller quantum computing modules. This is especially true for neutral atom systems, some trapped ion architectures and photonics-based approaches. Here we delve into the evaluation of various

methodologies for implementing optical interconnections between quantum processor modules to generate high-rate (> 10 kHz) photonic entanglement for neutral atom qubit species. Our work complements previous works on long-distance (~100 km) networking of processors[1–3] and specific schemes using a particular atom species.[4–8] This analysis aims to compare across disparate optical interconnect architectures to identify key enabling technologies and performance metrics needed, with particular attention to rubidium (^{87}Rb) and ytterbium (^{171}Yb) atoms.

We compare the following cases of optical interconnect schemes using several simple models:

1. State-of-the-art: Direct entanglement between individual atoms in two quantum computing modules (QCs).
    a. Coupling & Distance: Photon Starved // Photon Abundant Regime
2. Interconnects with intermediate memories
    a. Increase the rate of direct interconnects: photon-starved regime
    b. Entanglement scheduling
3. Multiplexed entanglement generation using channel and/or temporal multiplexing.
    a. Multiplexed entanglement rates (100 kHz-MHz)
    b. Requirement of an entanglement hub for networking in this regime
        i. Quantum memory
        ii. Switching and Routing
        iii. Bell state analyzers

2. Photonic entanglement schemes between neutral atom QC modules

2.1 State-of-the-art

Photonic entanglement schemes commonly employ communication qubits assigned for generating atom-photon entanglement. We consider the emissive regime of atom-photon entanglement generation since it is broadly applicable across qubit modalities. The communication qubits across two modules are simultaneously excited with an optical pulse. The atomic excitation results in spontaneous decay of the photon with its polarization or time-bin entangled with the resulting qubit state. The emitted photons are collected into high numerical aperture (NA) objective lenses or cavities, coupled to optical fibers and routed to a Bell-state-analyzer. The Bell state measurements result in a heralded entanglement based on the pattern of clicks at the detectors. In the case of polarization entangled photons the BSM setup consists of a non-polarizing beam splitter followed by polarizing beamsplitter (PBS) and 4 detectors (Fig. 1).

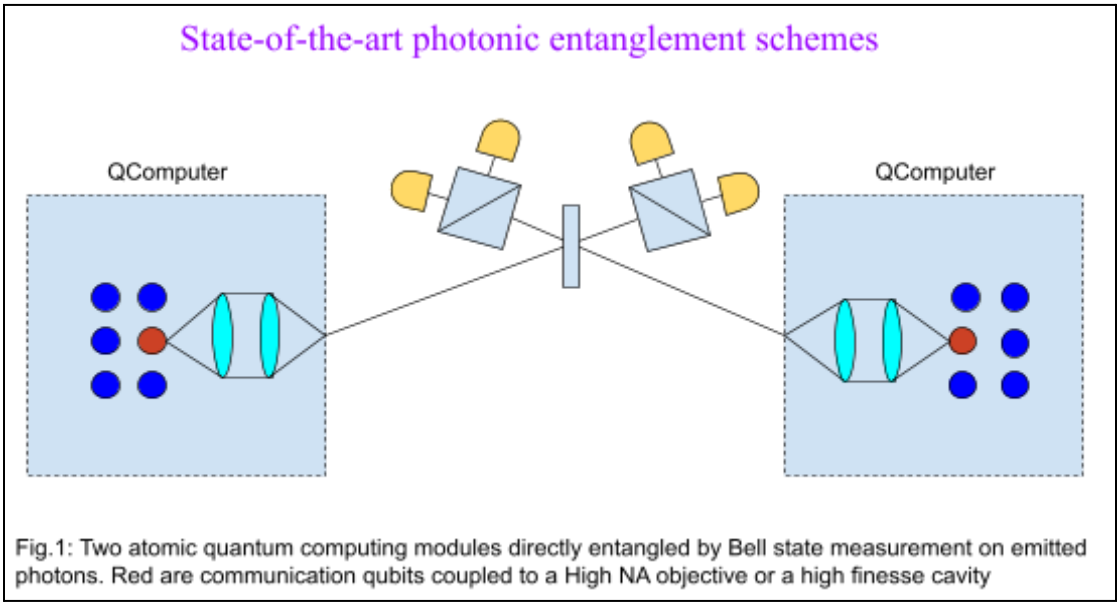

Fig.1: Two atomic quantum computing modules directly entangled by Bell state measurement on emitted photons. Red are communication qubits coupled to a High NA objective or a high finesse cavity

For a two-click based scheme such as time-bin, polarization encoding, the rate of atom-atom photonic entanglement is:

$$R = R_{attempt}\, p_s$$

where $R_{attempt}$ is the average Bell pair attempt rate (including cooling and initialization time), p_s is the average entanglement success probability per attempt defined as:

$$p_s = \eta_{BSM} p_i^2$$

Where p_i is photon detection probability from each individual atom and η_{BSM} is Bell state measurement success probability of 50% for polarization encoded photons since only 2 out of the 4 Bell states are heralded. The photon detection probability p_d is given as:

$$p_d = \eta_{collection} * \eta_{det} * \eta_{OE}$$

Where η_{det} is the detector efficiency, η_{OE} is the loss in optical components (off-chamber) and $\eta_{collection}$ is the total photon collection efficiency from the atom to fiber which depends on the specific photon collection schemes (e.g. free-space lens or cavity). The detector efficiency η_{det} is assumed to be 0.7.

We broadly classify the photonic entanglement into two regimes based on the rate of photon arrival from the two QPU into the BSM unit.

a) Photon starved regime

In this regime, a sparse stream of photons is received at the Bell-state measurement setup, which results in low entanglement rates ~Hz. A photon starved regime is primarily encountered in two scenarios:

- The first scenario where a low photon collection efficiency from the QPU (< 1%) results in a spare stream of photons with quadratically suppressed entanglement rates.

- The second scenario is over a long-distance (~100 km) networking of QPU the photon loss in the optical fiber (0.2 dB/km) can result in a photon starved regime.

b) Photon abundant regime
This regime is applicable for quantum networking in a data-center scale where under sufficiently high collection efficiency, the BSM units receive a steady stream of photons from the processors. In this regime, the entanglement generation between QPU can be near-deterministic.

2.1.1 Direct entanglement schemes

2.1.1 a) Free-space high NA objective lens

The photon collection efficiency in this case is defined as $\eta_{collection} = \eta_{atom\text{-}lens} * \eta_{lens\text{-}fiber}$ where $\eta_{atom\text{-}lens}$ is the photon collection efficiency of the lens and $\eta_{lens\text{-}fiber}$ is the photon coupling efficiency from the lens to a single mode fiber.

Demonstrations
A ^{87}Rb-^{87}Rb entanglement rate of 0.1 Hz was demonstrated over 6 km fiber[9] with entanglement success probability p_s = 3.66 x 10^{-6}. The total photon collection efficiency using a custom high NA objective lens $\eta_{collection}$ was ~ 0.01 and entanglement attempt rate $R_{attempt}$ was 30 kHz for a fiber distance of 6 km.
^{87}Rb-^{87}Rb entanglement rates as high as ~217 Hz have been proposed for attempt rate $R_{attempt}$ = 63 kHz by employing a high NA (0.7) objective lens with collection efficiency $\eta_{collection}$ of 0.12, an entanglement success probability p_s of 0.0035.[8]

2.1.1 b) Cavity enhanced photon collection

Photon collection efficiencies ($\eta_{collection}$) from the QC modules beyond the current limits of high NA lenses can be achieved by high-finesse optical cavities, either macroscopic (mm-cm scale), microcavities or nanophotonic cavities. The use of cavity can enhance the radiative decay of a particular transition through Purcell enhancement.
The photon collection efficiency into the cavity $\eta_{collection}$ depends on the cooperativity of the interaction (C) as[10] $\eta_{collection} \sim 2C/(2C+1)$.

Demonstrations
Table 1 below lists the different cavity modalities along with their collection efficiency, cooperativity and advantages. The details on each are discussed below.

SN	Cavity	C	$\eta_{collection}$	Advantages
1	Bulk Fabry-Perot[11] (FP) cavity	3	0.47	Simpler design.
2	Long near concentric cavity[4]	3	0.48	Trapping and cooling several atoms within the cavity mode, no requirement of atomic-transport.
3	Twisted-ring cavity[6] (^{171}Yb)	2.5	0.5	Large atom capacity (N~ 200) in the cavity mode supports multiplexing.

4	Fiber FP microcavity[12]	101	0.53	High cooperativity, optical access for atomic transport in optical tweezers[12].
5	Nanophotonic cavity[13] (^{171}Yb)	50	0.8	High cooperativity, on-chip photonic integration.
6	Nanofiber cavity[14] (^{171}Yb)	> 100	0.63	High cooperativity, large atom capacity (N~ 200) in the cavity mode supports multiplexing.

Table 1: Comparison of cavity modalities for networking neutral atoms. The atomic species is assumed to be ^{87}Rb unless specified. The cooperativity (C) corresponds to a single atom coupling to the cavity.

(i) Fabry-Perot bulk cavities: Entanglement between ^{87}Rb atoms in two separate cavities separated by 21 m was generated using a single photon transfer scheme.[11] The entanglement generation rate was 30 Hz, entanglement attempt rate was $R_{attempt}$ ~1.5 kHz, entanglement success probability p_s = 0.02. The primary limitation to p_s was a moderate cooperativity C of ~ 3, given the large cavity mode volume. The attempt rate of 1.5 kHz was limited by 100 µs of optical pumping and cooling, and the requirement of simultaneous atom localization at the center of the two cavities.

(ii) Long near-concentric cavities: Near-concentric FP cavities[4] exhibit smaller beam waist (5 µm) and longer cavity length (~20x) as compared to conventional FP cavities.[11] With cooperativity C ~3, mid-circuit ^{87}Rb state readout has been demonstrated using near-concentric cavities.[15] With an expected entanglement success probability p_s =0.056 ($\eta_{collection}$=0.48) and an attempt rate of $R_{attempt}$ ~ 57 kHz (10 µs cooling, 6 µs pumping), the projected Rb-Rb entanglement rate is 3.2 kHz.[4] A relatively longer mirror spacing (~10 mm) in long near-concentric cavities allows for trapping and cooling of atomic arrays within the cavity mode itself [2,4] without the requirement of atomic transport.

(ii) Fiber microcavities: Fiber Fabry-Perot microcavities (FFPC) have demonstrated strong atom-cavity coupling with cooperativity C ~ 100[12,16] and high collection efficiency $\eta_{collection}$ ~ 0.53.[17] Close proximity to the dielectric mirror surface (90 µm-160 µm[8,17]) in microcavities may require consideration of charge noise when the atom is excited to Rydberg states. However, recent works have demonstrated the compatibility of FFPC with optical tweezers based single atom transport[8] which will enable Rydberg excitations to be performed in a separate computation zone. Cavity mediated deterministic entanglement was recently demonstrated between two ^{87}Rb atoms in the same cavity.[12]

(iii) Photonic crystal cavity (PCC): Small mode volume and thus high cooperativity interaction with high collection efficiencies makes nanocavities ideal for deterministic long distance quantum networking. Targeting the telecom O-band metastable state transition in ^{171}Yb, prior work proposed coupling single ^{171}Yb atoms to a silicon PCC with high cooperativity (C~50) and photon collection efficiency ($\eta_{collection}$~0.8).[13]
Entanglement between ^{87}Rb atoms has been shown to be preserved during the transport of one of the atoms on a nanophotonic cavity.[18] The large time cost of shuttling (>0.65 ms[18]) makes time or spatial multiplexing necessary to achieve high entanglement generation rates. Recent works have

demonstrated integration of 64 optical tweezers with silicon chips hosting ~100 nanophotonic cavities and loading of multiple atoms on devices.[19]

(iv) Nanofiber cavity Individual atoms have been trapped on top of a nanofiber Fabry Perot cavity using a two-color guided mode trapping technique.[20] Recent works have also demonstrated the atomic trapping on nanofiber using optical tweezers, paving the way for individual atom manipulation on a nanofiber cavity.[14] A high cooperativity atom-cavity coupling[20] in nanofiber cavities makes them suitable for deterministic entanglement generation.

2.1.2 Comparing high-NA lens and cavity-based schemes

Table 2 below lists the proposed or measured entanglement rates for ^{87}Rb atoms with different optical readout modalities. Free-space high-NA lens and cavity based approaches have a proposed rate of 200 Hz and 3 kHz respectively with state-of-the-art measurements being at least 2 orders of magnitude lower, leaving room for improvements.

SN	Scheme	Measured/ Proposed	Attempt Rate	Entanglement Probability	Entanglement rates
1	High-NA lens[9]	Measured	30 kHz	3.66×10^{-6}	0.1 Hz
2	High-NA lens[8]	Proposed	63 kHz	3.5×10^{-3}	217 Hz
3	Near concentric cavity[4]	Proposed	57 kHz	0.056	3.2 kHz
4	FP bulk cavity[11]	Measured	1.5 kHz	0.02	30 Hz

Table 2: Proposed and measured photonic entanglement rates for ^{87}Rb with different optical readout schemes.

2.2 Quantum networking architectures for high-rate, high-fidelity photonic entanglement of QC modules

Generating high-rate, high-fidelity photonic entanglement across several quantum processor modules would require increasing the raw entanglement rates beyond 30 Hz, and developing hardware to implement a unified quantum networking layer over which entanglement can be scheduled across any pair of processors (Fig. 2).

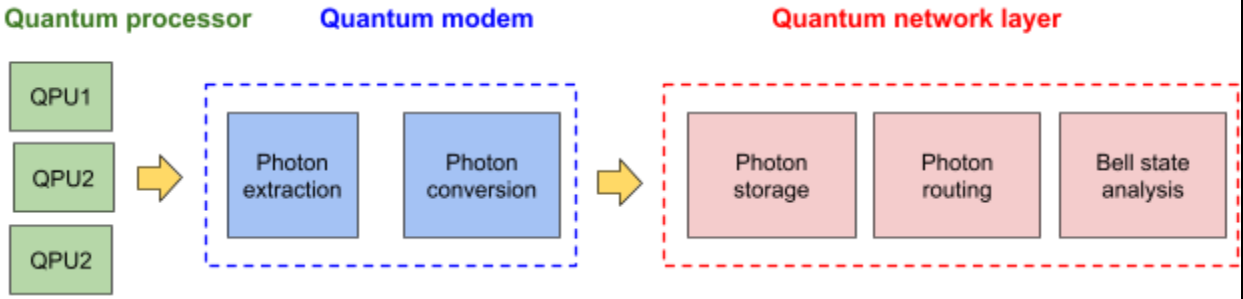

Fig.2: Architecture for entangling several quantum processing modules. Quantum modem refers to components aimed at increasing the photon extraction efficiency and converting the photons to appropriate wavelength/entanglement scheme to communicate with the quantum network layer. The quantum network layers contains quantum memories and arrays of switches, beamsplitters and detectors for scheduling entanglement across any processor.

1) Quantum networking layer: This layer serves as the central hub between different QPU modules, enabling communication between processors in a datacenter-scale setting as well as over a long-distance quantum network (red, Fig.2). The networking layer is implemented by components such as quantum memories, low-loss optical switches and Bell-state analyzers for entanglement storage, routing and heralding. We propose to use time-bin photonic entanglement modality for the quantum networking layer owing to its robustness over polarization-based entanglement schemes and compatibility with integrated photonics. Furthermore, telecom-C band wavelength (1.5 μm) is preferable for the quantum networking layer, owing to low propagation losses over optical fiber (0.2 dB/cm), as well as the availability of commercial optical components and integrated photonic design kits (PDKs).

1a) Photon storage: Time-bin quantum memories can be employed to store photons for scheduling asynchronous bell state measurements, effectively acting as a programmable/on-demand delay line. This capability is especially needed in the "photon starved" regime to increase the entanglement rate by synchronizing the sparse photon arrival events In this regime, the quantum memories would require coherence time commensurate with the mean arrival time between two photons from any QPU, and possess heralding capability, either intrinsic to the quantum memory or an external quantum non-demolition photon detector (QNDPD).

The primary role of quantum memory shifts from increasing entanglement rates in a low collection efficiency regime to entanglement scheduling in a high photon collection efficiency regime (photon abundant regime).

1b) Photon routing and Bell state analysis: Low-loss optical switches in conjugation with beam splitter and detector arrays can be employed to generate entanglement between any pairs of processors.

2) Quantum modem: Quantum modem layer interfaces the QPU to the quantum networking layer by 1) Enhancing photon collection from the QPU and 2) Converting photon entanglement basis and frequency (blue, Fig 2).

2a) Photon extraction: Components with on-chip elements such as cavities would be employed to increase the photon collection efficiency from atoms.

2b) Photon conversion: Polarization-based schemes typically achieve faster entanglement attempt rates compared to time-bin entanglement because they do not require additional qubit manipulation steps. For instance, in the case of $^{138}Ba^{+}$ ions, the time-bin scheme demonstrated 70 kHz[21] attempt rates while the polarization scheme had 1 MHz attempt rates.[22] Thus operating on a

photon polarization basis significantly accelerates entanglement attempt rates (14x speedup). However, propagating photon polarization qubits through optical components introduces complexities that can reduce entanglement rates and fidelity. These complexities include polarization-dependent losses and mixing in optical elements, as well as difficulties in creating polarization-agnostic photonic components. Our architecture leverages polarization based entanglement schemes to generate atom-photon entanglement in conjugation with polarization to time-bin basis converters[23] for interfacing with the quantum network. The basis converter is estimated to have a 3 dB loss, mainly due to EOM insertion losses. This polarization-to-time-bin conversion scheme is projected to achieve entanglement rates (~7x) higher than those obtained through purely time-bin entanglement techniques.

While photons in the time-bin entanglement basis are natively compatible with a variety of quantum memory modalities and are optimal for transmission over optical fibers, the optical frequency of many atomic transitions falls within the range of visible or visible-near infrared light, which yields prohibitively low transmission through standard optical fibers. As a result, implementation of frequency conversion to low-loss wavelength bands, like the telecom C-band would be needed. Beyond simple efficiency, this wavelength conversion step must also not introduce additional background photons that can develop due to Raman scattering or spontaneous parametric downconversion noise from external pump lasers. As a result, we are pursuing ultralow-noise solutions for optical transduction.[24]

2.3 Quantum Memory enabled asynchronous BSM between two QC modules

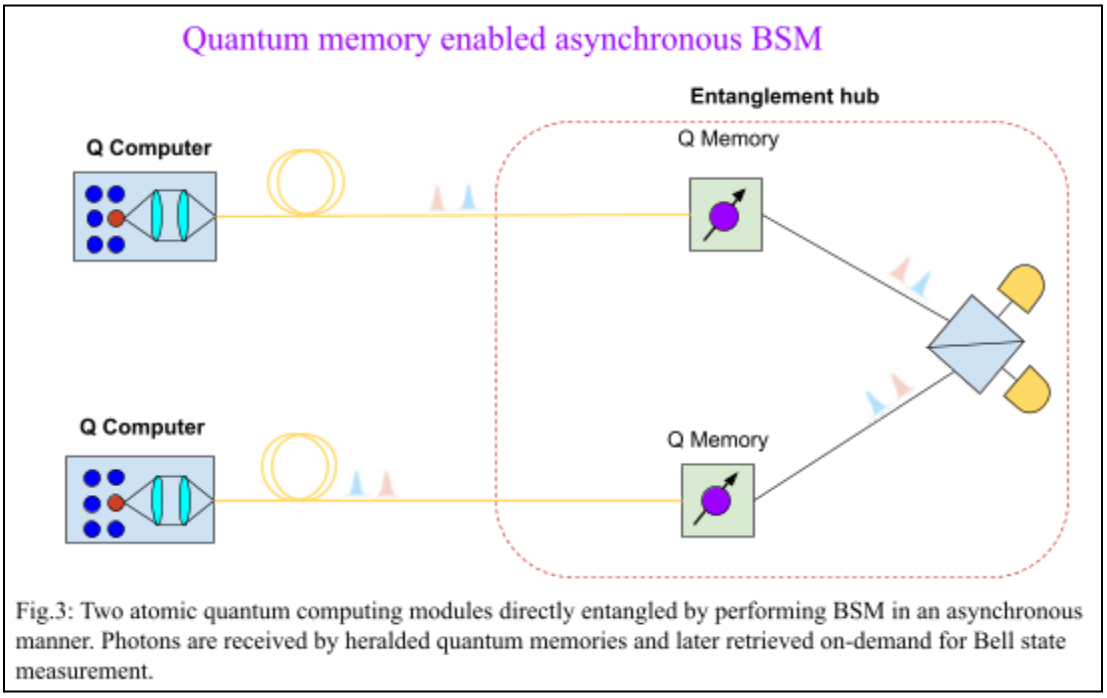

Fig.3: Two atomic quantum computing modules directly entangled by performing BSM in an asynchronous manner. Photons are received by heralded quantum memories and later retrieved on-demand for Bell state measurement.

Here we expand the state-of-the-art photonic entanglement schemes by adding a "catch-and-release" quantum memory as in interconnect. The direct BSM approach suffers from

the quadratic suppression of entanglement rate in a low photon collection efficiency regime. The photons emitted from the two modules have a low probability to arrive simultaneously in the low photon collection efficiency regime. A quantum memory relaxes the requirement of simultaneous photon arrival, thus changing the quadratic dependence on collection efficiency to a linear. This is analogous to the role played by quantum memories in a quantum repeater architecture.

The quantum memory for asynchronous BSM is required to be (i) on-demand (ii) multimode (temporal multiplexing) (iii) memory storage time needs to be longer than the time between the two photons from the communication qubits, typically up to ~ 3 ms (30 kHz entanglement attempt rate and 1% photon collection efficiency) (iv) broadband (>100 MHz) (v) wavelength matched.

2.3.1: Quantum memories for enhancing rates and scheduling entanglement

The two atomic qubits in the processors can be excited and photon can be extracted with a rate $R_{attempt}*\eta_{collection}$. The photon can be stored and later retrieved on demand from the memory with a total memory efficiency η_{mem}. Since the photon emission from each atom is a Poissonian distribution with a rate $R_{attempt}*\eta_{collection}$, the time interval between the subsequent photon emission from the two communication atom follows an exponential distribution with a rate $R_{attempt}*\eta_{collection}$. Thus, the rate of entanglement in with quantum memories will be proportional to the time between two subsequent photons from the two atoms:

$$R = \eta_{BSM} R_{attempt} * \eta_{collection} * \eta_{det}^{2} * (\eta_{mem}^{2} * F_{latency})$$

Where the factor $\eta_{mem}^{2}*F_{latency}$ captures the memory readout latency ($F_{latency}$) and efficiency (η_{mem}) from memory operation and η_{det} is the efficiency of detectors. The memory efficiency is defined as $\eta_{mem} = \eta_{herald}*\eta_{storage}*\eta_{FC}*\eta_{BW}$, where $\eta_{storage}$ is the storage & retrieval efficiency, η_{herald} is the heralding efficiency and η_{FC} and η_{BW} are frequency and bandwidth conversion efficiencies respectively. Since the rate of memory assisted entanglement is only linearly dependent on $\eta_{collection}$, obtaining $(\eta_{mem}^{2}*F_{latency}) > \eta_{collection}$ can provide an improvement in rates over direct entanglement by a factor ~ $(\eta_{mem}^{2}*F_{latency})/\eta_{collection}$ which is bounded by 100x for $\eta_{collection} \sim 0.01$.

Quantum memories can be functionally divided into two categories:

2.3.1 a) Heralded quantum memories:

These quantum memories herald the storage of incoming photonic qubits with an efficiency described by η_{herald}. The heralding aspect of the memory can be enabled by one of the three approaches:

- Inherent heralding, through a high cooperativity atom-cavity coupling, which results in phase shifts/reflection of the photon, conditional on the state of the memory qubit. Single color centers such as SiV^{-} strongly coupled to nanophotonic cavities have demonstrated heralded quantum memory [25]
- An external quantum non-demolition photon detector (nDPD) can be added before the quantum memory to add heralding capabilities. Rare-earth ion quantum memories have been demonstrated for non-demolition detection of photonic qubits. This scheme employs off-resonant phase shifts imparted by a time-bin qubit to a stored probe pulse[26].

- Entangled photon pair sources can be used to add heralding capabilities to absorptive quantum memories[27].

2.3.1 b) Non-heralded quantum memories:

Non-heralded quantum memories are standard catch-and-release quantum memories based on ensembles of cold atoms, warm vapor or rare-earth ions which do not have inherent heralding capabilities. While these memories may not boost the entanglement rates significantly (Appendix 1), the memory can operate as a programmable delay or on-demand delay line for scheduling entanglement.

Most absorptive quantum memory platforms such as vapor cells[28], trapped ion ensembles, rare-earth ion (REI) doped solids offer on-demand storage of time-bin[29]/polarization qubits [30] with high efficiency, bandwidth, storage time and fidelity. In particular, ^{87}Rb D_2 line ($^5S_{1/2}$, F=1 to $^5P_{3/2}$,F=0) at 780 nm used for photonic entanglement [4,9,11] matches well with ^{87}Rb cold ensemble-based quantum memories of polarization qubits. While these ensemble memories are non-heralded, efficiencies as high as 87%[31] for storage time of 10 μs have been reported. While we have primarily considered the memory efficiency, bandwidth and wavelength, additional considerations such as memory fidelity, storage time, noise, on-demand readout, should be taken into consideration while evaluating the suitability of a particular quantum memory for asynchronous BSM.

2.3.2 Comparing direct entanglement with quantum memory enhanced asynchronous BSM

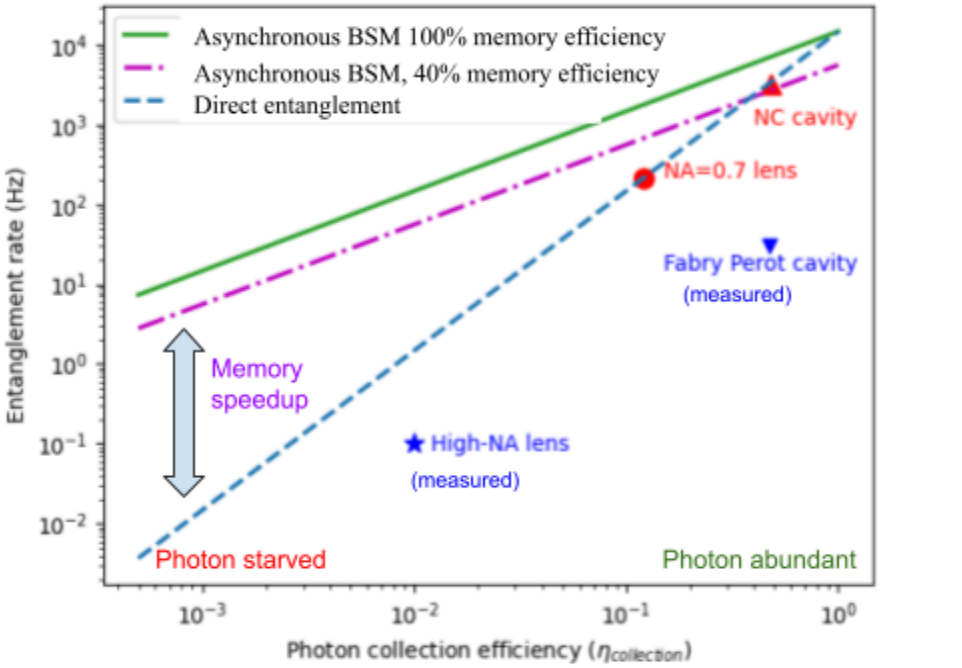

Fig. 4: Entanglement rate between two atoms as function of photon collection efficiency for ^{87}Rb (blue dashed line). Solid green line is a 100% memory efficiency while magenta dashed-dotted line is 40% memory efficiency. Blue stars and inverted triangles indicate measured ^{87}Rb atom-atom entanglement rates of 0.1 Hz with free-space scheme and ~ 30 Hz with macroscopic FP cavity, respectively. Red circle and triangle indicate proposed entanglement rates using high NA lens and near-concentric (NC) cavity respectively.

Figure 4 compares the direct entanglement rates with memory assisted asynchronous BSM for ^{87}Rb. Blue dashed lines represent the direct entanglement rates with red circle and triangle representing proposed rates using lens and cavity based schemes respectively. Solid green line indicates the case with 100% memory efficiency and magenta dashed-dotted line represents a memory with 40% efficiency. While quantum memories can improve entanglement rates by ~2 orders of magnitude in the low collection efficiency regime ($\eta_{collection} < 0.01$), state-of-the-art demonstrations exhibit high enough $\eta_{collection}$ to make improvements from asynchronous BSM marginal at best. Therefore, in a datacenter-scale, quantum memories would be primarily acting as a delay line for scheduling entanglement as opposed to enhancing entanglement rates. In contrast, over a long-distance quantum network (~10-100 km), photon loss from optical fiber would necessitate quantum memories to boost the entanglement rates, similar to quantum repeater schemes.

2.4 Multiplexed entanglement generation and routing

Multiplexing across multiple atoms can increase inter-module entanglement rates up to 100 kHz-MHz, higher than the rate ceiling of ~3-5 kHz for individual atoms. This can be implemented by a combination of temporal multiplexing to maximize the channel capacity and channel multiplexing to increase the number of parallel channels. Generating entanglement across any-to-any processor will require interfacing the processors with a quantum networking layer for efficient entanglement routing and scheduling. Fig. 5 below shows the architecture, with quantum processors interfaced with a central entanglement hub for quantum networking. The entanglement hub consists of 1) Quantum modems, for efficient photon extraction and conversion from processor 2) High efficiency multimode quantum memories to store photons for entanglement scheduling 3) Low-loss optical switches for photon routing, and 4) Photonic Bell state analyzers. Quantum modems are added at the processors for converting the emitted photons to a wavelength and an entanglement modality compatible with the quantum network.

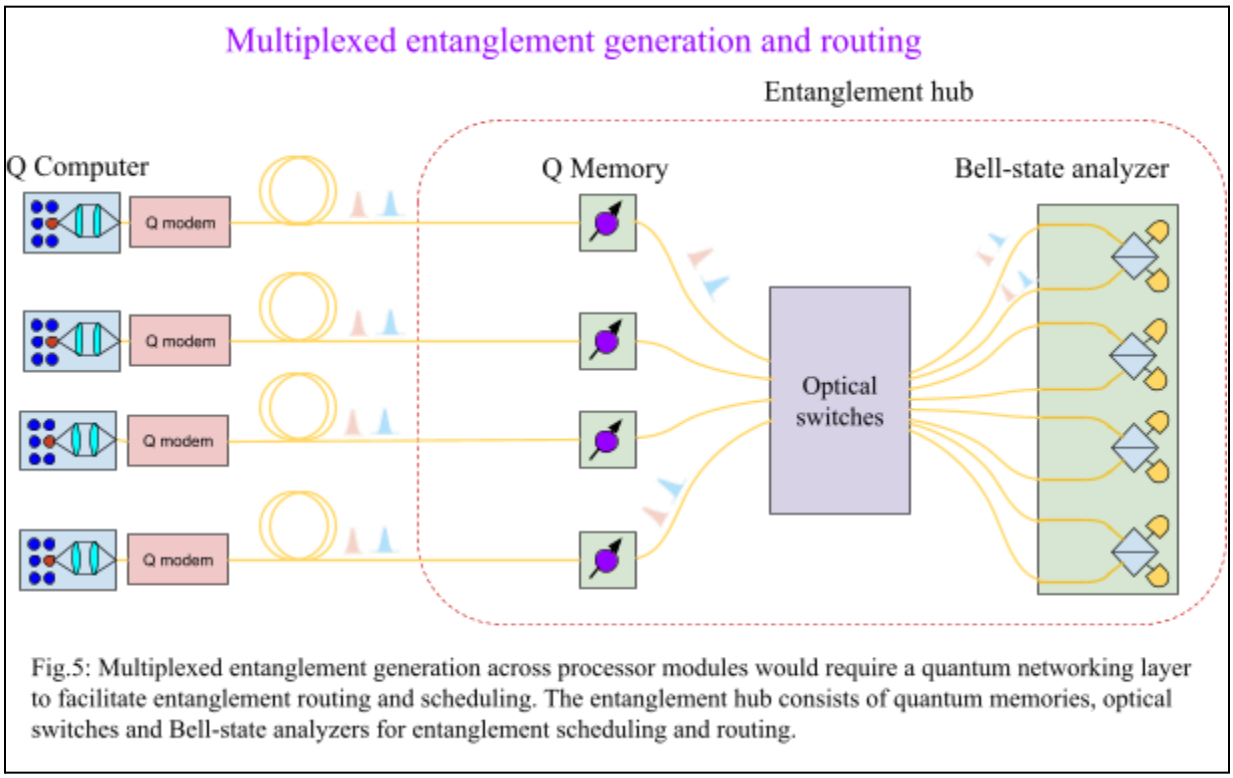

Fig.5: Multiplexed entanglement generation across processor modules would require a quantum networking layer to facilitate entanglement routing and scheduling. The entanglement hub consists of quantum memories, optical switches and Bell-state analyzers for entanglement scheduling and routing.

Temporal and channel multiplexing schemes for atom processor modules are outlined below:

(a) Temporal multiplexing: Temporal multiplexing is advantageous when the large time cost of atomic transport can be offset by sequential entanglement attempts across a large number of atoms loaded simultaneously in the cavity.[1] Sequential entanglement generation over the same optical readout channel also minimizes the physical infrastructure requirement. This approach requires (i) Loading multiple atoms simultaneously into the cavity/readout zone (ii) Ability to selectively address individual atoms by hiding the non-target atoms (e.g. site selective light shifts).

(b) Channel multiplexing (parallelization): Attempting entanglement on multiple atoms simultaneously i.e. spatial or channel multiplexing requires the ability to read out each individual atom through a separate channel and a separate set of BSM setup for each channel.

Table 2 summarizes the existing proposals on multiplexed entanglement generation on ^{171}Yb and ^{87}Rb coupled to cavities. All the proposals rely on some form of atomic transport to and from different zones, including loading and computation zones. The proposals (1-4) in Table. 1 are described below.

Both entries, #1[6] and #2[7] in Table 2 use the metastable $^3P_0$ to $^3D_1$ transition at 1389 nm as the readout. Proposal #1[6] uses twisted ring cavity to couple light from opposite helicity polarization into non-degenerate modes of the twisted ring cavity. Proposal #2[7] instead operates in time-bin entanglement schemes by coupling one one out of the 2 optical transitions from the qubit ground states with a nanofiber cavity. Both proposals expect ~ 100 kHz entanglement generation rates by temporally multiplexing ~ 200 atoms loading within a cavity. Site selective light shifts are proposed to be used for hiding the non-target atoms during sequential entanglement generation.

Entries #3,4 in the table from ref[8] coupled ^{87}Rb D_2 line transition to optical cavities. While #3 uses a large mode volume near-concentric cavity loaded with ~200 atoms to generate ~ MHz entanglements, #4 uses an array of 30 fiber microcavities to spatially multiplex entanglement generation.

#	Atom	Entanglement Scheme	Readout Scheme	Multiplexing Scheme	# of Atoms	Success probability	Entanglement rates
1	^{171}Yb	Polarization	Twisted ring cavity[6]	Temporal (sequential)	204	0.125	100 kHz
2	^{171}Yb	Time-bin	Nanofiber cavity[7]	Temporal (sequential)	200	0.2	100 kHz
3	^{87}Rb	Polarization	Near-concentric cavity[8]	Temporal (sequential)	160	0.1	1 MHz
4	^{87}Rb	Polarization	30-Fiber microcavity array[8]	Channel (parallel)	3 per cavity	0.24	~70 MHz

Table 3: Photonic entanglement rates for different multiplexing schemes proposed on neutral atoms.

Channel multiplexing would require arrays of Bell state analyzers and low-loss NxN optical switches to enable massive parallel operation. While temporal multiplexing lessens resource needs, its effectiveness could be improved by incorporating time-bin multiplexed quantum memories for entanglement scheduling. Both approaches would benefit from interfacing with a quantum networking layer at the central entanglement hub.

3. Conclusion

We analyze approaches to achieve high rate, high fidelity photonic interconnects between neutral atom QC modules. State-of-the-art photonic entanglement rates for ^{87}Rb are between 0.1 Hz with high-NA lens and 30 Hz with cavity-based schemes, with proposed improvement by ~100-1000x, up to 217 Hz with high-NA lens and 3-5 kHz with macroscopic cavities.

Asynchronous Bell state measurements with quantum memories could increase rates beyond direct entanglement in a low photon collection efficiency ($\eta_{collection}$~1%) regime by ~100x in the networking of neutral atom processors, where the effective entanglement rates are ~kHz. High efficiency quantum memories can be used as on-demand delay lines for scheduling entanglement generation in a high photon collection efficiency regime. Importantly, this advantage carries over at all network scales - cluster, campus and WAN.

Multiplexing across multiple atoms can provide inter-module entanglement rates in far excess of the ~kHz limit for individual atoms. Time multiplexing across N~200 atoms loaded in cavities has been proposed to achieve 100 kHz- MHz rates for both ^{87}Rb and ^{171}Yb. These approaches leverage the ability to trap ~100s of atoms in tweezer arrays and amortize the large cost of atom initialization and transport with time multiplexing. A multiplexed entanglement regime would require a quantum networking layer to facilitate efficient entanglement generation, routing and scheduling across several processor modules. The networking layer would be implemented by arrays of hardware components, which include 1) Quantum modems, 2) Quantum memories, 3) Low-loss optical switches, and 4) Bell state analyzers. memQ is developing these technologies to address the needs for quantum networking.

References

(1) Huie, W.; Menon, S. G.; Bernien, H.; Covey, J. P. Multiplexed Telecommunication-Band Quantum Networking with Atom Arrays in Optical Cavities. *Phys. Rev. Res.* **2021**, *3* (4), 043154. https://doi.org/10.1103/PhysRevResearch.3.043154.

(2) Covey, J. P.; Weinfurter, H.; Bernien, H. Quantum Networks with Neutral Atom Processing Nodes. *Npj Quantum Inf.* **2023**, *9* (1), 90. https://doi.org/10.1038/s41534-023-00759-9.

(3) Gu, F.; Menon, S. G.; Maier, D.; Das, A.; Chakraborty, T.; Tittel, W.; Bernien, H.; Borregaard, J. Hybrid Quantum Repeaters with Ensemble-Based Quantum Memories and Single-Spin Photon Transducers. arXiv 2024. https://doi.org/10.48550/ARXIV.2401.12395.

(4) Young, C. B.; Safari, A.; Huft, P.; Zhang, J.; Oh, E.; Chinnarasu, R.; Saffman, M. An Architecture for Quantum Networking of Neutral Atom Processors. *Appl. Phys. B* **2022**, *128* (8), 151. https://doi.org/10.1007/s00340-022-07865-0.

(5) Pattison, C. A.; Baranes, G.; Ataides, J. P. B.; Lukin, M. D.; Zhou, H. Fast Quantum Interconnects via Constant-Rate Entanglement Distillation. arXiv 2024. https://doi.org/10.48550/ARXIV.2408.15936.

(6) Li, Y.; Thompson, J. D. High-Rate and High-Fidelity Modular Interconnects between Neutral Atom Quantum Processors. *PRX Quantum* **2024**, *5* (2), 020363. https://doi.org/10.1103/PRXQuantum.5.020363.

(7) Sunami, S.; Tamiya, S.; Inoue, R.; Yamasaki, H.; Goban, A. Scalable Networking of Neutral-Atom Qubits: Nanofiber-Based Approach for Multiprocessor Fault-Tolerant Quantum Computer. arXiv 2024. https://doi.org/10.48550/ARXIV.2407.11111.

(8) Sinclair, J.; Ramette, J.; Grinkemeyer, B.; Bluvstein, D.; Lukin, M.; Vuletić, V. Fault-Tolerant Optical Interconnects for Neutral-Atom Arrays. arXiv 2024.

https://doi.org/10.48550/ARXIV.2408.08955.
(9) Van Leent, T.; Bock, M.; Fertig, F.; Garthoff, R.; Eppelt, S.; Zhou, Y.; Malik, P.; Seubert, M.; Bauer, T.; Rosenfeld, W.; Zhang, W.; Becher, C.; Weinfurter, H. Entangling Single Atoms over 33 Km Telecom Fibre. *Nature* **2022**, *607* (7917), 69–73. https://doi.org/10.1038/s41586-022-04764-4.
(10) Kobel, P.; Breyer, M.; Köhl, M. Deterministic Spin-Photon Entanglement from a Trapped Ion in a Fiber Fabry–Perot Cavity. *Npj Quantum Inf.* **2021**, *7* (1), 6. https://doi.org/10.1038/s41534-020-00338-2.
(11) Ritter, S.; Nölleke, C.; Hahn, C.; Reiserer, A.; Neuzner, A.; Uphoff, M.; Mücke, M.; Figueroa, E.; Bochmann, J.; Rempe, G. An Elementary Quantum Network of Single Atoms in Optical Cavities. *Nature* **2012**, *484* (7393), 195–200. https://doi.org/10.1038/nature11023.
(12) Grinkemeyer, B.; Guardado-Sanchez, E.; Dimitrova, I.; Shchepanovich, D.; Mandopoulou, G. E.; Borregaard, J.; Vuletić, V.; Lukin, M. D. Error-Detected Quantum Operations with Neutral Atoms Mediated by an Optical Cavity. arXiv 2024. https://doi.org/10.48550/ARXIV.2410.10787.
(13) Covey, J. P.; Sipahigil, A.; Szoke, S.; Sinclair, N.; Endres, M.; Painter, O. Telecom-Band Quantum Optics with Ytterbium Atoms and Silicon Nanophotonics. *Phys. Rev. Appl.* **2019**, *11* (3), 034044. https://doi.org/10.1103/PhysRevApplied.11.034044.
(14) Nayak, K. P.; Wang, J.; Keloth, J. Real-Time Observation of Single Atoms Trapped and Interfaced to a Nanofiber Cavity. *Phys. Rev. Lett.* **2019**, *123* (21), 213602. https://doi.org/10.1103/PhysRevLett.123.213602.
(15) Deist, E.; Lu, Y.-H.; Ho, J.; Pasha, M. K.; Zeiher, J.; Yan, Z.; Stamper-Kurn, D. M. Mid-Circuit Cavity Measurement in a Neutral Atom Array. *Phys. Rev. Lett.* **2022**, *129* (20), 203602. https://doi.org/10.1103/PhysRevLett.129.203602.
(16) Barontini, G.; Hohmann, L.; Haas, F.; Estève, J.; Reichel, J. Deterministic Generation of Multiparticle Entanglement by Quantum Zeno Dynamics. *Science* **2015**, *349* (6254), 1317–1321. https://doi.org/10.1126/science.aaa0754.
(17) Brekenfeld, M.; Niemietz, D.; Christesen, J. D.; Rempe, G. A Quantum Network Node with Crossed Optical Fibre Cavities. *Nat. Phys.* **2020**, *16* (6), 647–651. https://doi.org/10.1038/s41567-020-0855-3.
(18) Đorđević, T.; Samutpraphoot, P.; Ocola, P. L.; Bernien, H.; Grinkemeyer, B.; Dimitrova, I.; Vuletić, V.; Lukin, M. D. Entanglement Transport and a Nanophotonic Interface for Atoms in Optical Tweezers. *Science* **2021**, *373* (6562), 1511–1514. https://doi.org/10.1126/science.abi9917.
(19) Menon, S. G.; Glachman, N.; Pompili, M.; Dibos, A.; Bernien, H. An Integrated Atom Array-Nanophotonic Chip Platform with Background-Free Imaging. *Nat. Commun.* **2024**, *15* (1), 6156. https://doi.org/10.1038/s41467-024-50355-4.
(20) Kato, S.; Aoki, T. Strong Coupling between a Trapped Single Atom and an All-Fiber Cavity. *Phys. Rev. Lett.* **2015**, *115* (9), 093603. https://doi.org/10.1103/PhysRevLett.115.093603.
(21) Saha, S.; Shalaev, M.; O'Reilly, J.; Goetting, I.; Toh, G.; Kalakuntla, A.; Yu, Y.; Monroe, C. High-Fidelity Remote Entanglement of Trapped Atoms Mediated by Time-Bin Photons. arXiv 2024. https://doi.org/10.48550/ARXIV.2406.01761.
(22) O'Reilly, J.; Toh, G.; Goetting, I.; Saha, S.; Shalaev, M.; Carter, A.; Risinger, A.; Kalakuntla, A.; Li, T.; Verma, A.; Monroe, C. Fast Photon-Mediated Entanglement of Continuously-Cooled Trapped Ions for Quantum Networking. arXiv 2024. https://doi.org/10.48550/ARXIV.2404.16167.
(23) Hodges, J.; Pappas, S.; Weinstein, Y.; Gilbert, G. Polarization/Time-Bin Basis Conversion of Entangled Photons. In *Conference on Lasers and Electro-Optics 2012*; OSA: San Jose, California, 2012; p QF3F.3. https://doi.org/10.1364/QELS.2012.QF3F.3.

(24) Agha, I.; Davanço, M.; Thurston, B.; Srinivasan, K. Low-Noise Chip-Based Frequency Conversion by Four-Wave-Mixing Bragg Scattering in SiN_x Waveguides. *Opt. Lett.* **2012**, *37* (14), 2997. https://doi.org/10.1364/OL.37.002997.
(25) Bhaskar, M. K.; Riedinger, R.; Machielse, B.; Levonian, D. S.; Nguyen, C. T.; Knall, E. N.; Park, H.; Englund, D.; Lončar, M.; Sukachev, D. D.; Lukin, M. D. Experimental Demonstration of Memory-Enhanced Quantum Communication. *Nature* **2020**, *580* (7801), 60–64. https://doi.org/10.1038/s41586-020-2103-5.
(26) Sinclair, N.; Heshami, K.; Deshmukh, C.; Oblak, D.; Simon, C.; Tittel, W. Proposal and Proof-of-Principle Demonstration of Non-Destructive Detection of Photonic Qubits Using a Tm:LiNbO3 Waveguide. *Nat. Commun.* **2016**, *7* (1), 13454. https://doi.org/10.1038/ncomms13454.
(27) Liu, X.; Hu, J.; Li, Z.-F.; Li, X.; Li, P.-Y.; Liang, P.-J.; Zhou, Z.-Q.; Li, C.-F.; Guo, G.-C. Heralded Entanglement Distribution between Two Absorptive Quantum Memories. *Nature* **2021**, *594* (7861), 41–45. https://doi.org/10.1038/s41586-021-03505-3.
(28) Mottola, R.; Buser, G.; Treutlein, P. Optical Memory in a Microfabricated Rubidium Vapor Cell. *Phys. Rev. Lett.* **2023**, *131* (26), 260801. https://doi.org/10.1103/PhysRevLett.131.260801.
(29) Wei, S.-H.; Jing, B.; Zhang, X.-Y.; Liao, J.-Y.; Li, H.; You, L.-X.; Wang, Z.; Wang, Y.; Deng, G.-W.; Song, H.-Z.; Oblak, D.; Guo, G.-C.; Zhou, Q. Quantum Storage of 1650 Modes of Single Photons at Telecom Wavelength. *Npj Quantum Inf.* **2024**, *10* (1), 19. https://doi.org/10.1038/s41534-024-00812-1.
(30) England, D. G.; Michelberger, P. S.; Champion, T. F. M.; Reim, K. F.; Lee, K. C.; Sprague, M. R.; Jin, X.-M.; Langford, N. K.; Kolthammer, W. S.; Nunn, J.; Walmsley, I. A. High-Fidelity Polarization Storage in a Gigahertz Bandwidth Quantum Memory. *J. Phys. B At. Mol. Opt. Phys.* **2012**, *45* (12), 124008. https://doi.org/10.1088/0953-4075/45/12/124008.
(31) Cho, Y.-W.; Campbell, G. T.; Everett, J. L.; Bernu, J.; Higginbottom, D. B.; Cao, M. T.; Geng, J.; Robins, N. P.; Lam, P. K.; Buchler, B. C. Highly Efficient Optical Quantum Memory with Long Coherence Time in Cold Atoms. *Optica* **2016**, *3* (1), 100. https://doi.org/10.1364/OPTICA.3.000100.

Appendix 1:

Asynchronous Bell State measurement rates for a non-heralded memory.

The entanglement attempt cycle is repeated over a long enough time t. The emitted photons from the two communication qubits are stored in two separate memories during this storage cycle lasting for a time *t*. Finally, the two memories are read out at the same time, on-demand. In this case, while the calculation of entanglement rates are similar to the derivation above, there is a penalty on rates. In the lack of a heralding signal, there is an additional reduction in rates, due to the cases where either/both of the two atoms don't decay into the memory during the storage cycle. This can be captured by a factor ($\eta_{unherald}$).
Assuming the capture time $t \sim 1/R_p$, where R_p is the photon collection rate from individual atom, we get:

$$\eta_{unherald} = P_{(ion\ doesn't\ decay)}{}^2 = (1-1/e)^2 \sim 0.4$$

Thus, an unheralded memory will capture one photon from each of the two atoms about 40% of the time during the storage cycle, resulting in reduction of entanglement rates by a factor $\eta_{unherald}$

$$R = (\eta_{BSM} R_{attempt} p * \eta^2 * F_{latency}) * \eta_{unherald}$$